

Cloud microphysics, radiation and vertical velocities in two- and three-dimensional simulations of deep convection

By VAUGHAN T. J. PHILLIPS^{1*} and LEO J. DONNER²

¹*Princeton University, USA*

²*Geophysical Fluid Dynamics Laboratory, Princeton, USA*

(Received 15 August 2005; revised 7 August 2006)

SUMMARY

This study investigates the importance of dimensionality for the characteristics of simulations performed with cloud-system resolving models (CSRMs). In addition to intrinsic questions related to dimensionality in CSRMs, the issue has gained added interest since CSRMs can be utilized instead of conventional cloud parametrizations to represent deep convection within global climate models. Such CSRMs may be either two- or three-dimensional.

CSRM simulations of five observed cases of deep convection are performed in both two and three dimensions (2D and 3D) with the aim of elucidating the impact of dimensionality on overall cloud statistics. Observed profiles of the large-scale average of advection of temperature and humidity are applied to initiate and maintain the convection. Two of the cases are from tropical oceanic regions. The other three cases are continental.

The average ascent rate in deep convective, cloudy updraughts is about 20–50% higher at mid-levels of the troposphere in 3D than in 2D, for all cases. This corresponds to an increase by a similar percentage in the vertical mass flux of deep updraughts in the oceanic cases. Furthermore, the weak ascent ($0.1 < w < 1 \text{ m s}^{-1}$) outside the deep convective updraughts is much less prevalent in 3D than in 2D, with vertical velocities being about 20% lower for a given cumulative frequency and a lower vertical mass flux. Downdraughts are weaker in 3D, for most cases.

There is a substantial sensitivity of the vertical profiles of cloud liquid and cloud ice, and of other microphysical species, to dimensionality. This is consistent with the sensitivity of the dynamics of convection. Corresponding changes in radiative transfer, especially in the short-wave band, result from the cloud–radiative interactions. In particular, the peak in domain-averaged cloud liquid content in the melting layer is about 50% higher in most of the 2D simulations. The land cases display more sensitivity of the short-wave radiative flux to the choice of orientation of the vertical plane of 2D simulations.

KEYWORDS: Cloud–radiation interactions Cloud-system resolving model

1. INTRODUCTION

Throughout the history of development of cloud-system resolving models (CSRMs), fundamental dynamical differences have been apparent in cloud simulations with different dimensionalities. Updraughts were found to be faster in three dimensions (3D) compared with two dimensions (2D) (e.g. Wilhelmson 1974; Tag and Rosmond 1980; Schlesinger 1984; Lipps and Hemler 1986; Tao *et al.* 1987; Redelsperger *et al.* 2000), whereas downdraughts were generally weaker. The sensitivity to dimensionality was linked to differing characteristics of the inflowing air (Wilhelmson 1974) and vertical pressure-gradient force (Schlesinger 1984).

2D CSRMs have been widely applied to the study of deep convection because of their minimal computational expense compared with 3D models (e.g. Held *et al.* 1993; Grabowski *et al.* 1996). Cloud statistics or mass budgets have been claimed to be quite similar between 2D and 3D in some CSRM studies (e.g. Grabowski *et al.* 1998; Xu *et al.* 2002). By contrast, Donner *et al.* (1999) found that the third dimension caused the free troposphere to be warmer by up to 1 K on average and less humid. Radiative heating destabilized the mesoscale stratiform region to a greater extent in 3D than in 2D, producing warmer temperatures. Petch and Gray (2001) also found that the third dimension produced a more intense anvil circulation. Tompkins (2000) concluded that, for random or scattered convection, the profiles of moisture and temperature diverged

* Corresponding author: Department of Meteorology, University of Hawaii, Honolulu, USA.
e-mail: vaughanp@hawaii.edu

© Royal Meteorological Society, 2006.

after a few days between 3D and 2D for CSRMs with the same number of grid points. Simulations of the boundary layer have revealed differences in the properties of turbulence between 2D and 3D (Moeng *et al.* 1996).

Cloud microphysics might also be expected to be affected by dimensionality, since cloud dynamics and microphysics are intimately related (e.g. Cotton and Tripoli 1978). Ascent of updraught parcels leads to condensation and eventually can cause the freezing of condensate. The rate of ascent influences the balance between warm and cold processes of precipitation formation by determining whether there is enough time for coagulation of cloud particles to occur and whether supercooled cloud liquid can survive in the presence of ice (e.g. Heymsfield *et al.* 2005; Phillips *et al.* 2006). Aggregation of crystals is a slow process favoured by weak ascent. Redelsperger *et al.* (2000) found that the faster updraughts in 3D reached colder temperatures, causing a greater production of ice aloft. The supersaturation, which determines rates of nucleation of cloud particles, is determined by the intensity of ascent. The stratiform melting layer is another example of the tight coupling between cloud dynamics and microphysics (e.g. Findeisen 1940; Wexler *et al.* 1954; Atlas 1955; Atlas *et al.* 1969; Riehl 1977; Stewart *et al.* 1984; Willis and Heymsfield 1989).

In addition to such considerations of the intrinsic effects from the third dimension on clouds, the issue of dimensionality has been highlighted by recent attempts to install a CSRm within each grid column of a global model (Grabowski and Smolarkiewicz 1999; Grabowski 2001; Khairoutdinov and Randall 2001). The CSRm replaces conventional parametrizations of convective and stratiform cloud, with which it compares favourably (e.g. Su *et al.* 1999; Xie *et al.* 2002).

The aim of the present paper is to explore differences between 2D and 3D CSRm simulations of vertical velocity, mass flux, and the microphysical and radiative properties of clouds. The type of analysis here aims to add to previous studies by the use of:

- a range of cases in three geographic regions;
- a wide range of dynamical, microphysical and radiative quantities from the simulations, in comparison with observations;
- equalized numbers of grid points between the ensembles of 2D runs and the corresponding 3D runs in order to minimize differences in variability arising from differences in grid size.

Two of the geographic regions simulated are oceanic, their locations being the eastern Atlantic (30 August–19 September 1974) for GATE* and the western Pacific (20–26 December 1992) for TOGA-COARE†. The third region is continental: central Oklahoma for subcases A (27 June–1 July 1997), B (8–12 July 1997) and C (13–17 July 1997) of the ARM‡ Program. Results are discussed in section 3 for these cases. Conclusions are presented and discussed in section 4.

2. DESCRIPTION OF THE CLOUD-SYSTEM RESOLVING MODEL AND THE EXPERIMENTAL SET-UP

(a) Numerical model

The CSRm utilized here is the Weather Research and Forecasting (WRF) model. A general description of how the compressible non-hydrostatic equations are solved in

* The GARP (Global Atmospheric Research Program) Atlantic Tropical Experiment.

† The Tropical Ocean/Global Atmosphere–Coupled Ocean/Atmosphere Response Experiment.

‡ Atmospheric Radiation Measurement.

WRF has been given by Michalakes *et al.* (2001). The time-integration scheme for WRF is a third-order Runge–Kutta-based time-splitting technique and has been described by Wicker and Skamarock (2002). There is a high time-resolution integration of acoustic waves in addition to the ordinary time integration for the resolved flow. Further details are available from http://wrf-model.org/documentation_main.html.

The Eulerian-height dynamical core was selected for this paper. This core makes use of a terrain-following height coordinate. The planetary boundary-layer (PBL) scheme is that of the medium-range forecast model of the National Centers for Environmental Prediction described by Hong and Pan (1996), with a countergradient flux for heat and moisture. The PBL height is computed from a critical bulk Richardson number. Vertical diffusion is represented with an implicit local scheme, based on the local Richardson number in the free troposphere. A subgrid-scale horizontal diffusion scheme based on K -theory is applied, where K is constant. Surface fluxes of heat and moisture are calculated using similarity theory. Stability functions from Paulson (1970), Dyer and Hicks (1970) and Webb (1970) are applied to evaluate the surface-exchange coefficients.

The version of the Lin *et al.* (1983) microphysics scheme described by Lord *et al.* (1984) was implemented. It has five classes of hydrometeor (cloud liquid, cloud ice, snow, graupel and rain) and includes sedimentation of cloud ice. The saturation adjustment scheme proposed by Lord *et al.* is also included. Empirical data from Heymsfield and Donner (1990) for the terminal velocity of ice crystals was applied to include cloud ice in the precipitation flux.

The Geophysical Fluid Dynamics Laboratory (GFDL) radiation code was also incorporated (Freidenreich and Ramaswamy 1999; Schwarzkopf and Ramaswamy 1999). The radiative effects of aerosols and non-CO₂ trace gases were neglected. Clouds were treated as absorbers in the long-wave with non-grey absorption coefficients in eight spectral bands. The single-scattering properties in the solar spectrum are those of Slingo (1989) for cloud liquid, Savijarvi (1997) for rain, Fu and Liou (1993) for cloud ice and Fu *et al.* (1995) for snow. In the long-wave spectrum, the single-scattering properties are those of Held *et al.* (1993) for cloud liquid, Fu *et al.* (1995) for rain and snow, and Fu and Liou (1993) for cloud ice. These scattering properties are evaluated as functions of the corresponding contents of microphysical species predicted by the microphysics parametrization in WRF. Graupel was treated radiatively in the same manner as snow. The generalized effective particle sizes of cloud droplets and snow are 20 μm and 150 μm , respectively, while those of cloud ice and rain are given by empirical functions of height (McFarquhar *et al.* 1999) and rainwater content (Savijarvi *et al.* 1997), respectively. The diurnal cycle of radiation is fully implemented. The radiative fluxes are evaluated once every 10 min.

A sponge layer is applied aloft with a strength of $\kappa_0(z - z_0)$, where $z_0 = 14$ km above mean sea level (MSL) and $\kappa_0 = 2 \times 10^{-6} \text{ m}^{-1} \text{ sec}^{-1}$, following Donner *et al.* (1999) (see also Held *et al.* 1993). The sponge damps the potential temperature to observations, instead of to the horizontal means.

(b) Design of experiments

In these experiments, WRF is integrated with a 2 km horizontal resolution and a 500 m vertical resolution. The vertical grid has 40 levels. A time step of 10 sec is used. The standard size of the horizontal domain in 2D is 170 km (85 grid points) long and in 3D is 170 \times 170 km². All lateral boundary conditions are periodic for all prognostic variables.

For each case of convection simulated there are two ensembles of 2D runs and one 3D simulation. Each 2D ensemble consists of 85 members and each member is 85 grid points long, equalizing the total number of grid points with the corresponding 3D simulation. In one of the two ensembles, all 2D members are in the zonal plane ('2D(X)'); in the other, all are in the meridional plane ('2D(Y)'). Ensemble members were initialized with unique sets of random perturbations of the vapour mixing ratio in the boundary layer obtained from the corresponding 3D run. For each ensemble, the 2D fields were then averaged across all members ('the 2D(X) and 2D(Y) simulations') for comparison with the 3D run. Additionally, the averaging was done by merging both ensembles (the '2D[(X + Y)/2] simulation').

To explore whether the area for upward and downward motions affects the convective dynamics in 2D, an extra run with a large domain that is 4800 km (2400 grid points) long in the zonal plane was performed for TOGA-COARE only. The number of grid points in this 'long-domain 2D run' is a third of that in the 3D run. (Memory limitations prevented the number of grid points being equalized between the two runs). The similarity of vertical-velocity statistics from the long-domain 2D run with results from corresponding 2D ensembles (section 3) did not warrant its application to other cases.

Profiles of observed temperature and moisture are from Thompson *et al.* (1979) for GATE, Ciesielski *et al.* (1997) for TOGA-COARE, and Zhang and Lin (1997) and Zhang *et al.* (2001) for ARM. Perturbations are imposed on the initial field of vapour mixing ratio to initiate convection following Donner *et al.* (1999) and Lipps and Hemler (1986). For the oceanic cases, the observed time-series of sea surface temperature (SST) was used. For the land cases, observed surface fluxes of heat and moisture were applied.

Tendencies representing the domain-averaged advection of potential temperature and vapour mixing ratio (e.g. Grabowski *et al.* 1996; Donner *et al.* 1999) are from Thompson *et al.* (1979) for GATE, from Ciesielski *et al.* (1997) for TOGA-COARE and from the constrained variational analysis for ARM (Zhang and Lin 1997; Zhang *et al.* 2001). Also, the domain average of the horizontal wind was relaxed towards observed values on a timescale of 1 hour (e.g. Grabowski *et al.* 1996).

During the first few hours of the simulated period of TOGA-COARE, the presence of cloud in the mid or upper troposphere was apparent from the observation that the outgoing long-wave radiation (OLR) was substantially lower than the value expected from clear-sky emission. Zero precipitation was observed. The dilemma was how to represent the radiative effects of the initial cloud in the CSRM, as there were no observations either of its properties in situ or of its large-scale advection into the domain. As the cloud was non-precipitating, the most parsimonious assumption is that it continued to be advected into the domain throughout the simulated period, being uniformly persistent in the background. It may have been part of a widespread cloud-deck originating from a remote source. Although the observed initial sounding of water vapour was anomalously dry (the relative humidity with respect to ice, RH_i , was less than about 60% at all subzero levels), all subsequent soundings throughout the simulated period were quite moist at most subzero levels with $RH_i > 80\text{--}90\%$ (section 2(c)). This is consistent with the above assumption that the initial non-precipitating cloud persisted for the entire simulated period. Observational limitations prevent a direct representation of the microphysical quantities. Instead, an attempt is made solely to represent its radiative effects by adding a fixed increment to the cloud-ice mixing ratio that is passed as an input to the radiation code for the entire duration of the simulation. The increment of cloud-ice mixing ratio was selected so as to match the predicted radiative fluxes with

those observed in the Minnis/IMET* (see Burks 1998) dataset at the start of the TOGA-COARE run, a uniform value of about 0.02 g kg^{-1} over the layer 6–9 km above MSL and zero at all other altitudes. This perturbation was applied only to the radiation code and only in the TOGA-COARE simulations.

A 2D simulation was performed without any offset representing the persistent non-precipitating cloud ('the no-initial-ice simulation'). At the top of the atmosphere, the no-initial-ice run produced errors in the downward short-wave and outgoing long-wave radiative fluxes of about -60 and 30 W m^{-2} , respectively, when averaged over the entire simulation. The corresponding errors from the first hour or so are about -200 and 50 W m^{-2} , respectively. The persistence of the initial errors throughout the no-initial-ice simulation is consistent with the above assumption that the initial non-precipitating cloud persisted for the whole simulated period of TOGA-COARE, at least over some portion of the simulated domain.

(c) *Observed characteristics of cases*

The oceanic and land cases differed in the observed characteristics as follows:

- the peaks of mid-tropospheric cooling by large-scale advection were more intense in the land cases than in the oceanic ones;
- precipitation events were heavier in the land cases than in the oceanic ones;
- the deep shear of the horizontal mean flow was stronger for TOGA-COARE and ARM(A) than the other cases (as shown in Fig. 1), whilst the shear during GATE was sometimes moderate and sometimes weak;
- the relative humidity in the free troposphere is much higher in the oceanic cases than in the land ones, especially for TOGA-COARE at upper levels (for instance, at 5 km above MSL the relative humidity with respect to water is usually about 30–60% in the land cases and 50–80% in the oceanic cases, and at 10 km above MSL the relative humidity with respect to ice is usually about 50–90% for GATE, 80–100% for TOGA-COARE and 20–70% for the land cases).

3. RESULTS FROM 2D VERSUS 3D COMPARISON

(a) *Vertical motions associated with deep convection*

The vertical-velocity structures differ strongly between 2D and 3D, with higher values of vertical velocity in 3D. Figure 2 displays height–time cross-sections of vertical velocity conditionally averaged over cloudy† updraughts $> 1 \text{ m s}^{-1}$ for an oceanic case (GATE). On average, updraught speeds in deep convection are higher in 3D than in 2D by about $1\text{--}2 \text{ m s}^{-1}$ at mid levels. The maximum of average updraught speed is usually located in or near the lower half of the mixed-phase region (5–8 km above MSL). The temporal evolution of vertical velocity is similar to that found in the other cases.

Figure 3 shows the profiles of vertical velocity conditionally averaged over cloudy updraughts $> 1 \text{ m s}^{-1}$, as before, for all cases. At mid levels (i.e. 5–10 km above MSL), the average updraught speed is about 20–50% higher in 3D than in 2D in most cases. The greatest sensitivity with respect to dimensionality is found in the upper troposphere over 10 km above MSL. In the land cases, the peak in average updraught speed at 14–16 km above MSL is about three times as high in 3D as in 2D, while the maximum

* Improved METeorology—a programme for measurements from ship and buoy systems.

† Combined mixing ratio for cloud liquid and cloud ice $> 0.1 \text{ g kg}^{-1}$.

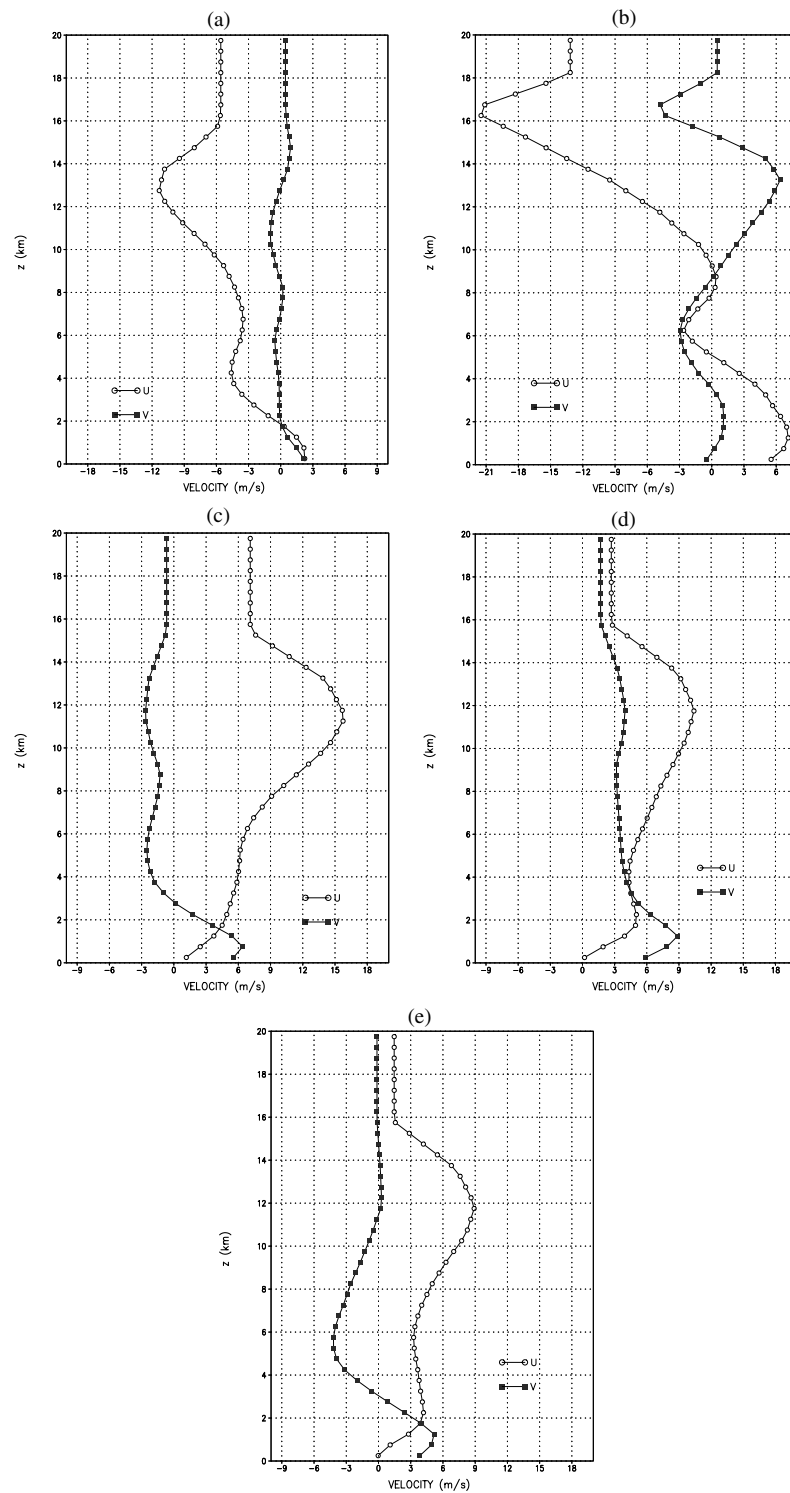


Figure 1. Profiles of zonal, U , and meridional, V , components of the observed horizontal mean flow (m s^{-1}), time-averaged over the simulated periods of (a) GATE, (b) TOGA-COARE, (c) ARM(A), (d) ARM(B) and (e) ARM(C).

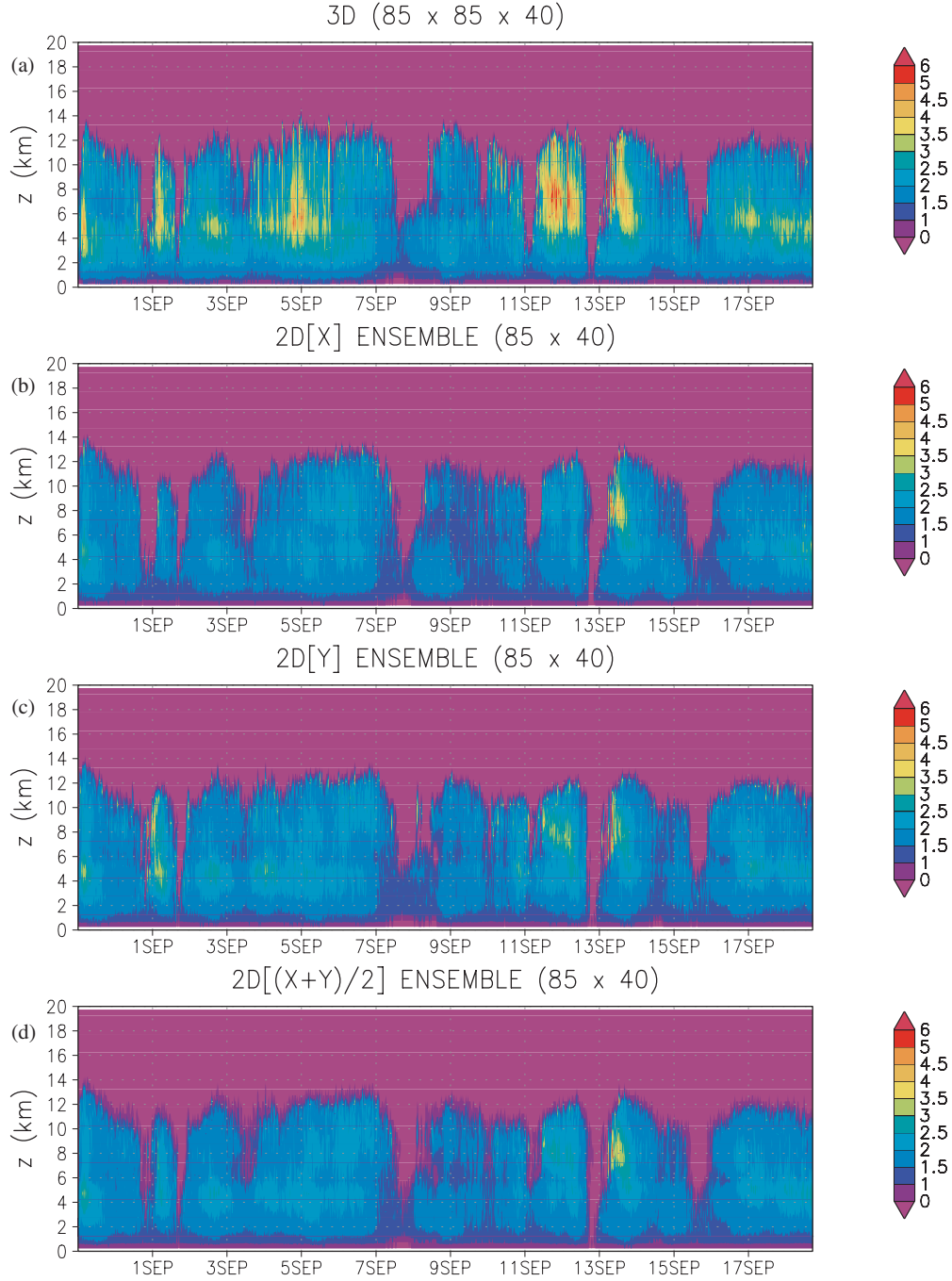


Figure 2. Ascent in cloudy updrafts for GATE in (a) the 3D run and in the 2D ensembles (b) 2D(X), (c) 2D(Y) and (d) 2D[(X + Y)/2]. The conditional averaging is performed over points where the vertical velocity exceeds 1 m s^{-1} and the the cloud mixing ratio is at least 0.1 g kg^{-1} .

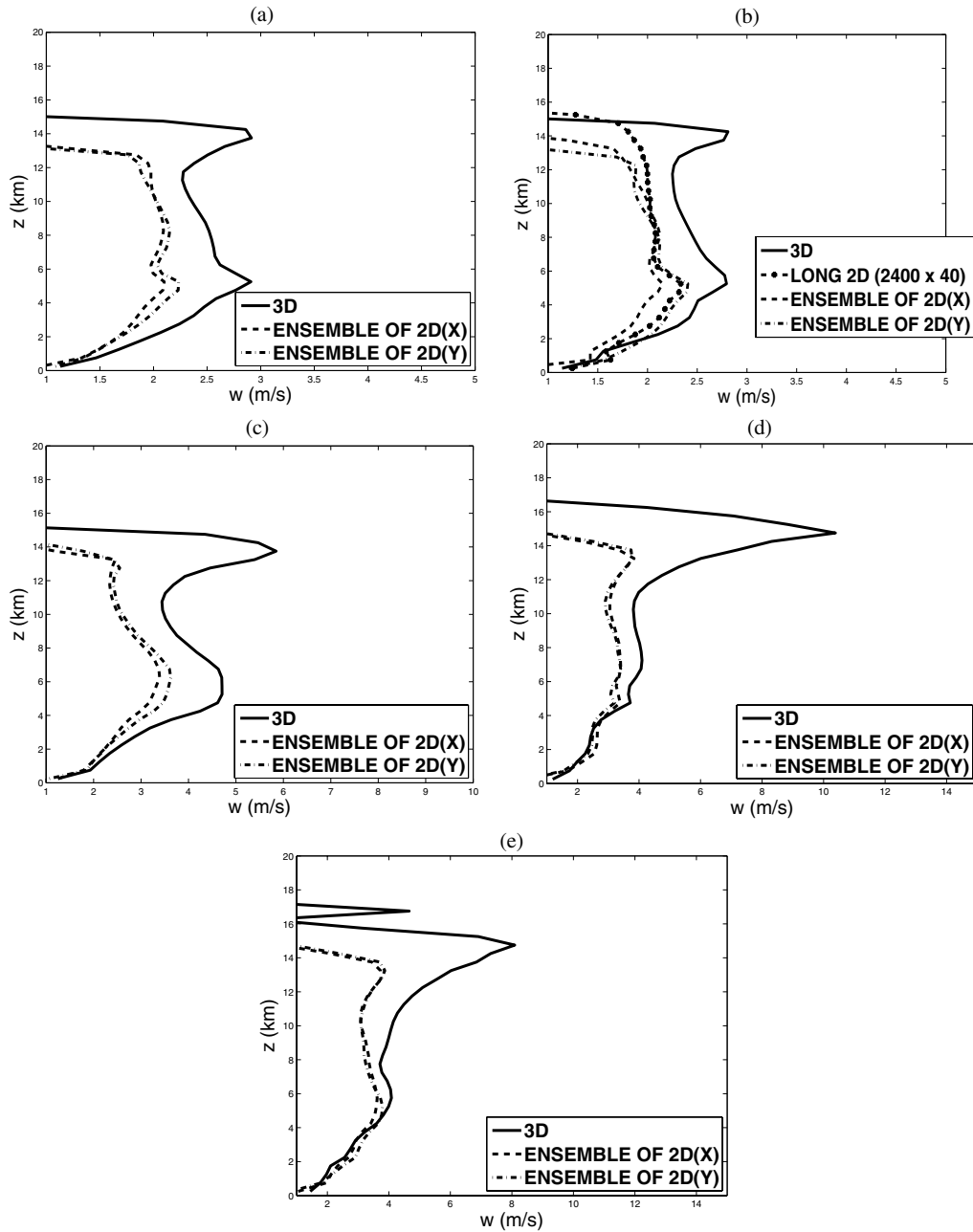


Figure 3. Time-averaged profiles of vertical velocity in cloudy updrafts $> 1 \text{ m s}^{-1}$ for (a) GATE, (b) TOGA-COARE, (c) ARM (A), (d) ARM (B) and (e) ARM (C) in the 3D run and the 2D ensembles.

level reached by these cloudy updraughts is 1–2 km higher. This sensitivity is more pronounced than for the oceanic cases.

Figure 4 displays a comparison with aircraft observations (LeMone and Zipser 1980) of the predicted histogram of vertical velocities within cloudy updraughts of deep convection between 4 and 8 km above MSL in GATE. Observations are only available for this particular range of altitudes. Generally, the predicted 3D histogram agrees well with aircraft observations over most of the range of observed frequencies, while the 2D simulations consistently underpredict the vertical velocity. For all cases, the histograms show that deep convective updraughts are faster in 3D than in 2D. Vertical velocities in the most vigorous 1% of updraughts are about 3 to 4 m s⁻¹ (20–40%) higher in most cases in 3D relative to 2D. The difference between 2D(X) and 2D(Y) simulations is much less than that between 2D and 3D simulations, in all cases.

Figure 5 shows histograms for the full vertical-velocity distribution throughout the whole domain in regions of ascent and descent at levels above 2 km above MSL. Again, intense updraughts are generally faster in 3D than in 2D. However, in most cases (except for TOGA-COARE), the ‘weak ascent’ ($0.1 < w < \sim 1$ m s⁻¹) outside the rapid convective updraughts is less prevalent in 3D, with vertical velocities being about 20% lower for a given cumulative frequency, relative to 2D. Downdraughts are about 20% faster at each cumulative frequency in 2D compared with 3D. TOGA-COARE is again an exception, as it must be given its more frequent ascent at almost all vertical velocities. Only levels higher than 8 km above MSL contribute to the weak ascent being more prevalent in 3D than in 2D for TOGA-COARE.

Also shown in Figs. 3, 4 and 5 are results from the long-domain 2D run (2400 grid points) for TOGA-COARE. These are very similar to the corresponding profiles and histograms from the 2D ensembles. The impact from increasing the domain size is minimal compared with that obtained from changing the dimensionality.

Figure 6 provides an example of how the vertical-velocity histograms for the whole domain are related to vertical mass fluxes. It indicates the vertical mass flux in GATE across the whole domain for regions (both cloudy and cloud-free) of deep (> 1 m s⁻¹) and weak (< 1 m s⁻¹) ascent, and for all regions of descent. For deep ascent, mass fluxes are higher in 3D by about 20% and 30–50% at most levels in GATE and TOGA-COARE, respectively, whereas in the land cases (not shown) they are lower by about 20% due to cloud-free deep ascent being less prevalent, relative to 2D. The mass flux of deep convective updraughts was 10% higher in the 3D simulations of TOGA-COARE undertaken by Petch and Gray (2001) than in 2D, which is qualitatively similar to the sensitivity found with WRF. For weak ascent, mass fluxes are lower in 3D than in 2D at most levels by about 20% in all cases, relative to 2D, except for ARM(C) where they are about 10% lower and for TOGA-COARE where they are slightly greater higher than 8–10 km above MSL. Despite deep convective updraughts having higher vertical velocities in 3D than in 2D, there is actually slightly less subsidence across the whole domain in 3D in all cases, except for TOGA-COARE where there is slightly more subsidence over 8–10 km above MSL, relative to 2D.

(b) *Microphysics*

Figure 7 shows the vertical profiles of mixing ratios of cloud ice, cloud liquid, graupel, snow, and rain, unconditionally averaged over the whole domain for GATE. Stratiform cloud provides the dominant contribution to the average mixing ratio of cloud liquid at levels between the surface and the anvil. In this case, and in all other simulations (not shown), there is a pronounced maximum in the mixing ratio of cloud liquid just below the freezing level (about 4–5 km above MSL). The maximum is caused

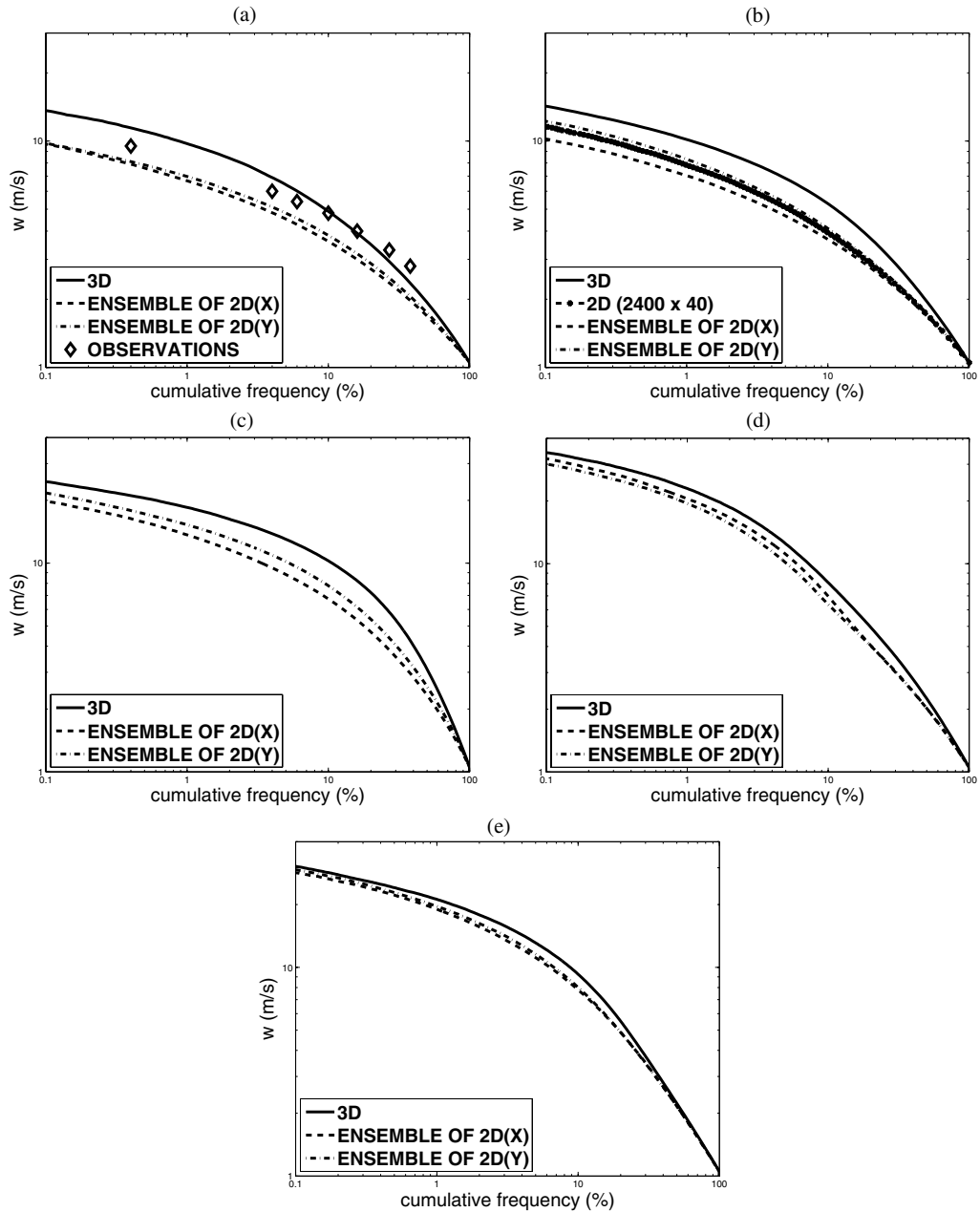


Figure 4. (a) Cumulative frequency distribution of vertical velocity in the cloudy updraughts $> 1 \text{ m s}^{-1}$ between 4 and 8 km above MSL in GATE in the 3D run and the 2D ensembles, compared with aircraft observations. Also shown are similar plots, but without observations, for (b) TOGA-COARE (together with the long-domain 2D run), (c) ARM (A), (d) ARM (B) and (e) ARM (C).

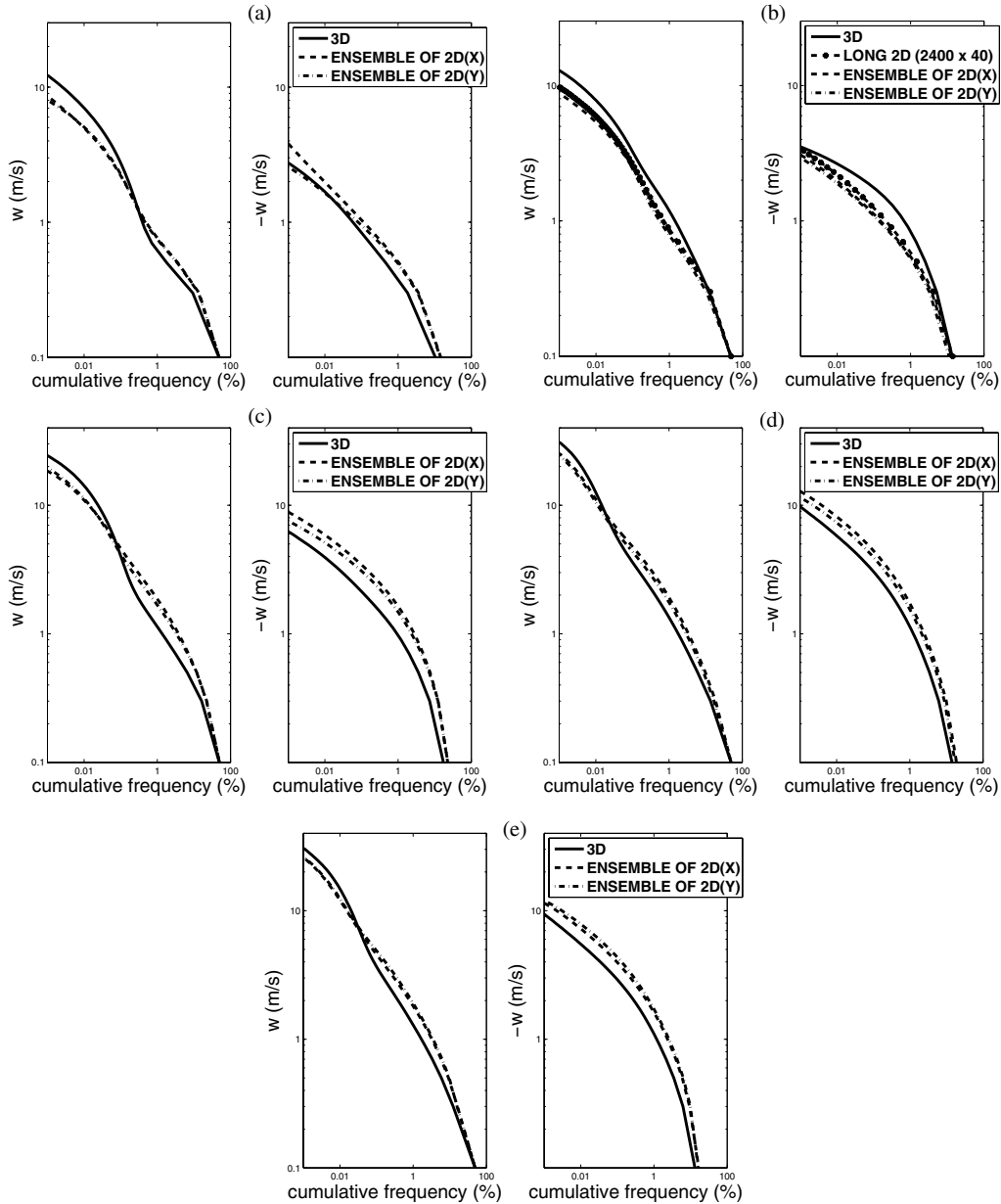


Figure 5. Cumulative frequency distribution of vertical velocity ($|w| > 0.1 \text{ m s}^{-1}$) for all ascent (left-hand panels) and all descent (right-hand panels) across the whole domain between 2 and 8 km above MSL for (a) GATE, (b) TOGA-COARE, (c) ARM (A), (d) ARM (B) and (e) ARM (C) in the 3D run and the 2D ensembles.

by production of stratiform cloud associated with the minimum of equivalent potential temperature predicted in the melting layer (see sections 1, 3(c) and 4).

Table 1 shows the sensitivity to dimensionality of the peak values of mixing ratio for the various microphysical species in all cases. In both oceanic cases, the peak of cloud liquid mixing ratio is about 50% higher in 2D than in 3D. The cloud liquid mixing ratio at subzero temperatures is similarly sensitive. This sensitivity to dimensionality is

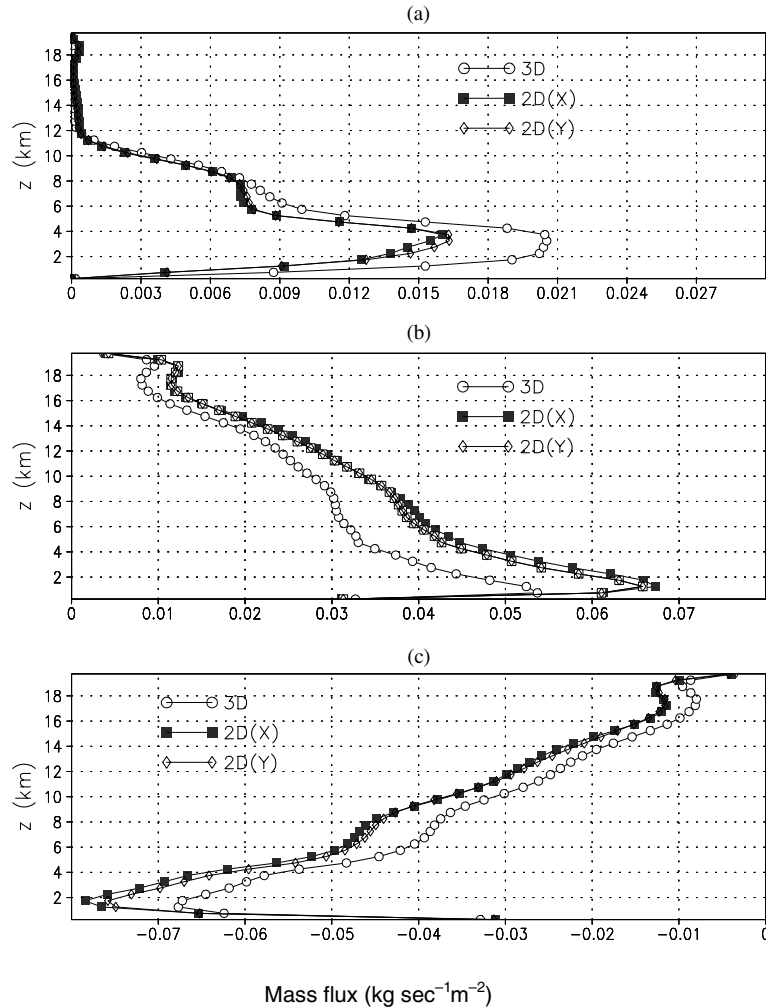


Figure 6. Vertical mass flux ($\text{kg sec}^{-1} \text{m}^{-2}$) for GATE unconditionally averaged across the whole domain (a) for rapid ascent ($w > 1 \text{ m s}^{-1}$) and (b) for weak ascent ($0 < w < 1 \text{ m s}^{-1}$) ascent, and (c) for descent ($w < 0 \text{ m s}^{-1}$) in the 3D run and the ensembles 2D(X) and 2D(Y).

consistent with the mass flux of weak ascent ($< 1 \text{ m s}^{-1}$), which drives condensation at low levels, being higher in 2D compared with 3D and boosting the formation of stratiform cloud. The land cases (especially ARM (C)) less clearly follow this pattern, which reflects the complex interactions of differing wind shears and environmental humidity with processes governing its formation and dissipation and the deep convective cells that detrain into stratiform cloud.

Generally, the peak in mixing ratio of cloud ice at 8–10 km above MSL is about 10–70% higher in 2D than in 3D in all cases. The snow mixing ratio is higher by a similar percentage in all cases in 2D, partly because production of stratiform cloud is greater in most cases, and the slow process of snow production (section 1) is expected to be more significant in stratiform cloud than in deep convection. Also, a greater mass of crystals is available for snow formation by aggregation in 2D. There is a greater mass of supercooled cloud-liquid aloft for the growth of snow by riming in most cases.

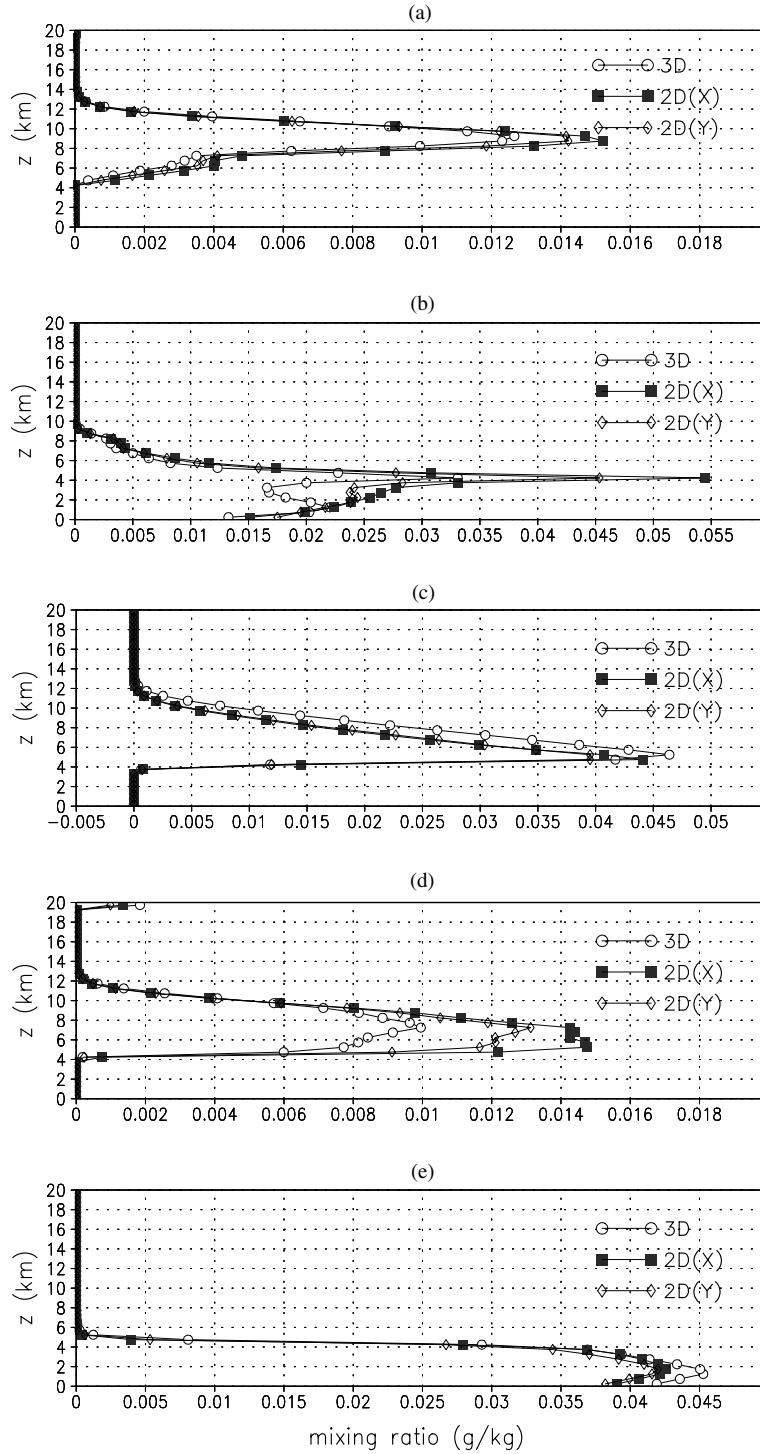


Figure 7. Microphysical species for GATE unconditionally averaged across the whole domain: (a) cloud-ice, (b) cloud liquid water, (c) graupel, (d) snow and (e) rain in the 3D run and the ensembles 2D(X) and 2D(Y).

TABLE 1. RATIO OF THE 2D AND 3D PEAK DOMAIN-AVERAGED CONTENTS OF MICROPHYSICAL SPECIES FOR GATE, TOGA-COARE AND ARM

Case	Simulation	Microphysical species				
		Cloud-liquid	Cloud-ice	Graupel	Snow	Rain
GATE	2D(X)/3D	1.69	1.25	0.95	1.49	0.94
	2D(Y)/3D	1.39	1.19	0.86	1.33	0.93
TOGA-COARE	2D(X)/3D	1.56	1.09	0.84	1.18	1.00
	2D(Y)/3D	1.47	1.11	0.81	1.32	0.89
	2D(long-domain)/3D	1.18	1.06	0.88	1.17	0.94
ARM(A)	2D(X)/3D	1.64	1.67	1.14	1.82	1.22
	2D(Y)/3D	1.11	1.19	0.88	1.30	0.85
ARM(B)	2D(X)/3D	0.89	1.16	0.91	1.23	0.86
	2D(Y)/3D	1.54	1.16	0.93	1.49	1.01
ARM(C)	2D(X)/3D	0.93	1.16	0.90	1.32	0.97
	2D(Y)/3D	0.60	1.05	0.93	1.09	0.86

The graupel mixing ratio is lower by about 10–20% in 2D than in 3D at most subzero levels in all cases (except for the 2D(X) ARM(A) run, which also has a correspondingly high ratio of supercooled cloud liquid and cloud ice). In 3D, the higher vertical velocities of deep convection cause more rain to be upwelled above the freezing level for conversion to graupel prior to melting and fallout. More graupel is then lifted to higher altitudes by more intense ascent, so it accretes more cloud liquid, accumulating still more mass. The sensitivity of the average rain mixing ratio to dimensionality of the simulations is low.

The mixing ratio of vapour (not shown), averaged over the entire domain, is lower in 2D throughout the free troposphere relative to 3D, by up to about 10–20% and 20–30% in the oceanic and land cases, respectively. The percentage difference is typically greatest at about 10–14 km above MSL. For the long-domain 2D simulation of TOGA-COARE, the average mixing ratio of vapour throughout most of the free troposphere is about 5 to 10% drier relative to 3D and up to about 5% drier relative to 2D(X). Large-scale organization of convection causes a drying of the mean state in the long-domain 2D WRF run. The humidity of the boundary layer is insensitive to dimensionality in the WRF simulations. Qualitatively, these results are consistent with those from 2D runs of varying lengths of Tompkins (2000) and/or Petch and Gray (2001).

In the oceanic cases, the domain-averaged temperature is colder by up to about 1 K throughout the free troposphere in the 2D(X) and 2D(Y) simulations, with the greatest cooling located at about 10–12 km above MSL, relative to 3D. This is similar to the sensitivity found by Donner *et al.* (1999) (section 1). In the land cases, the sensitivity of the domain-averaged temperature is more ambiguous: the lower (<5 km above MSL) and upper (>10 km above MSL) troposphere tend to be warmer than in 3D by up to about 0.2–0.6 K, while the mid troposphere is more similar, relative to 3D. For the long-domain 2D simulation of TOGA-COARE, the average temperature is warmer throughout the troposphere by <0.3 K relative to 3D, which is qualitatively similar to the sensitivity found by Tompkins (2000), and by about 0.4 K at all levels relative to 2D(X). In GATE, the time-averaged ratio of condensate to vapour (not shown) displays a maximum value at 14 km above MSL that is almost 20% higher in 3D than in 2D.

(c) *Phase-change heating rates*

Figure 8 shows the contribution from stratiform cloud (defined as the region outside deep convection where the total liquid-water path exceeds 0.2 kg m^{-2} , with the criteria of Xu 1995) to the domain-averaged heating and cooling rates associated with condensation and melting, respectively, for 2D(X) and 3D simulations of GATE. Condensation rates are generally much higher in 2D than in 3D at most levels below the freezing level. There are maxima of condensation in the melting layer located at about 4.2–4.5 km above MSL, being linked to the peak in cloud liquid mixing ratio (see section 3(b)). During episodes of intense condensation, the regions of enhanced condensation rate tend to extend downwards from the melting layer to almost 1 km above MSL, especially in 2D.

Maxima in the rate of melting are collocated temporally and spatially with maxima of condensation rate in the melting layer, especially in 2D. Most of the ice falling out melts over a narrow layer (4.2–4.5 km above MSL). However, the layer of complete melting (about 3.5–4.5 km) is predicted to be much deeper than this, as is typically seen in aircraft observations (e.g. Willis and Heymsfield 1989). Also, the intensity of most maxima in the melting rate is about 20% higher in 2D than in 3D, owing to more stratiform cloud in and below the melting layer.

Figure 9 depicts the profiles of equivalent potential temperature (θ_e) for GATE, conditionally averaged on isothermal surfaces over regions inside water-saturated stratiform cloud. The vertical coordinate is the height of data points on each surface, averaged in the same manner to facilitate comparison with other plots presented here. The predicted profile of θ_e is qualitatively in agreement with profiles derived from aircraft observations (e.g. Stewart *et al.* 1984; Willis and Heymsfield 1989) and displays a minimum at 4.2 km above MSL about 300 m below the freezing level. As was seen in aircraft observations by Stewart *et al.* (1984), this minimum in θ_e is located at the base of the narrow layer within which most of the mass of ice melts due to latent cooling from melting. Above the minimum in θ_e , the local troposphere is convectively stable ($\partial\theta_e/\partial z > 0$). Below it, the ambient cloudy air is unstable ($\partial\theta_e/\partial z < 0$). Such stable layers in and above the melting layer decouple the unstable layers below it from those at higher levels (e.g. Moore and Stewart 1985).

The minimum in θ_e is about 2 degC colder in 2D than in 3D. Consequently, destabilization of stratiform areas below the melting layer appears to be substantially more pronounced in 2D, the lapse rate of θ_e being almost 100% steeper at 1–4 km above MSL than in 3D. The lapse rate of θ_e is a measure of the degree of potential convective instability of moist atmospheric layers. This is the same range of altitudes where condensation rates are much higher in 2D than in 3D (Fig. 8), as noted above. It is consistent with the greater production of stratiform cloud found in 2D, which was also evident from the predicted profiles of cloud liquid mixing ratio (see section 3(b)).

(d) *Radiation*

Table 2 shows the upward and downward components of the radiative flux at the top (TOA) and base (SFC) of the atmosphere, respectively, for the 2D and 3D simulations of GATE, TOGA-COARE and ARM. The upward TOA component of the short-wave flux is higher for most 2D simulations than in 3D, by up to 20 W m^{-2} , due to more reflection of solar radiation from higher amounts of stratiform cloud liquid and, to a lesser extent, from more anvil cloud ice (Table 1). This causes the downward SFC component of the short-wave flux to be correspondingly lower in 2D than in 3D. In most cases, these responses are less applicable to 2D(Y) short-wave fluxes because the profile of cloud

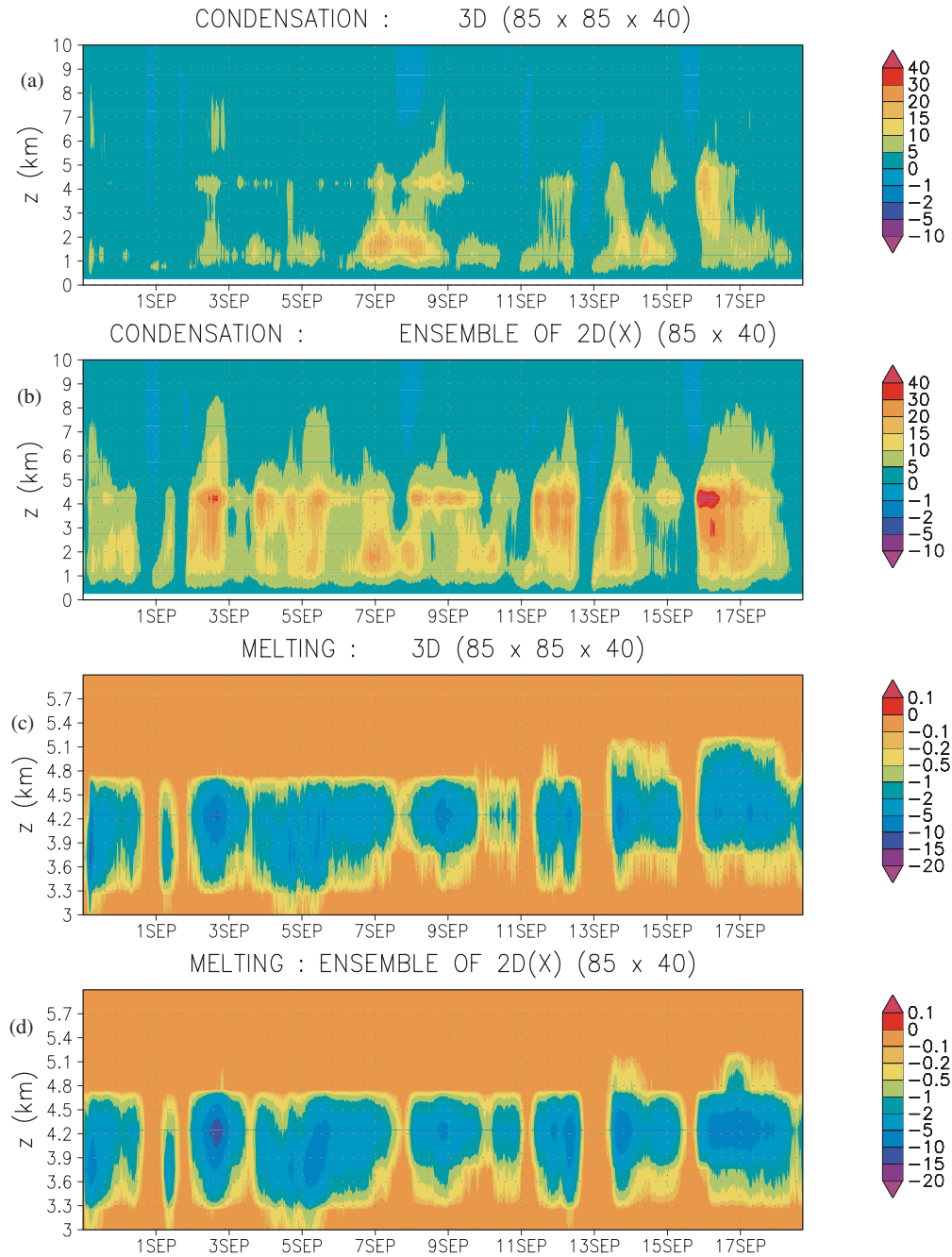


Figure 8. The contribution to domain-wide rates of latent heating (K day^{-1}) from condensation and melting for atmospheric columns containing stratiform cloud in the GATE 2D(X) and 3D simulations.

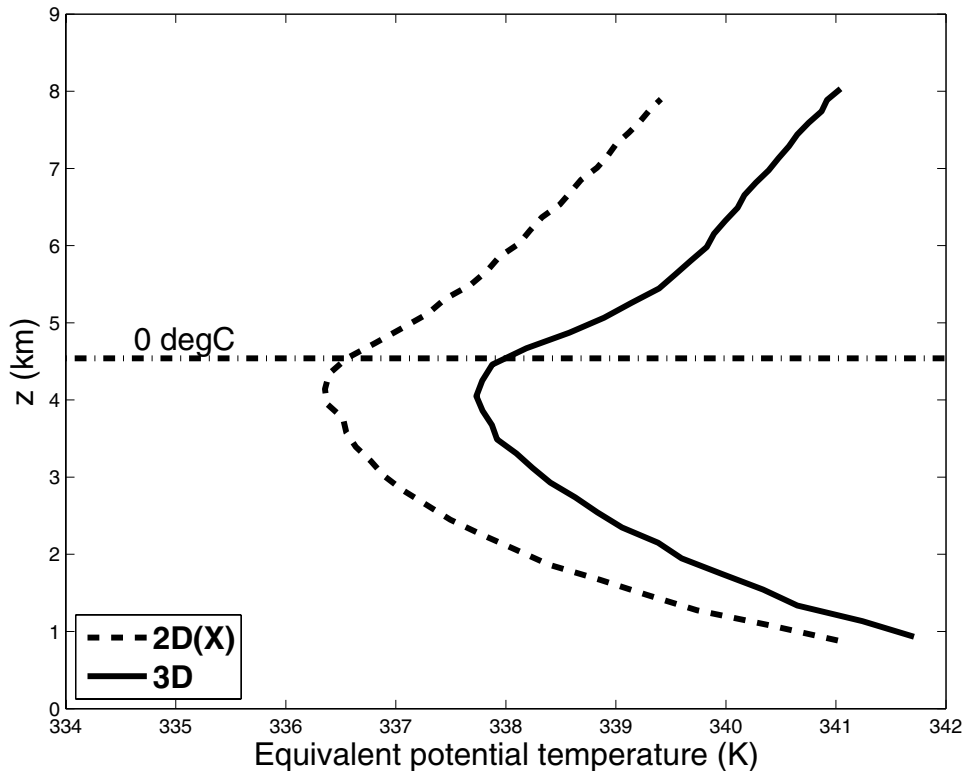


Figure 9. Vertical profiles of equivalent potential temperature conditionally averaged on isothermal surfaces inside water-saturated stratiform cloud, from GATE in the 2D(X) and 3D simulations.

liquid mixing ratio less clearly follows that pattern. The difference between 2D(Y) and 3D short-wave fluxes is less than that between 2D(X) and 2D(Y), in all cases other than GATE. The land cases display a much greater difference of the short-wave fluxes between 2D(X) and 2D(Y) simulations than the oceanic cases. The wind shear has an impact on the stratiform peak of cloud liquid in 2D. The land cases have a much lower relative humidity than the oceanic cases in the free troposphere (section 2(c)), which reduces the distance over which the mean flow can transport condensate away from convective cores before its removal by evaporation and sublimation.

The sensitivity of the predicted long-wave flux to dimensionality is less than that of the predicted short-wave fluxes, indicating that low clouds dominate the sensitivity to dimensionality. Extensive middle cloud absorbs much of the long-wave radiation emitted by the earth's surface, becoming radiatively saturated and limiting the effect of changes in the coverage and microphysical properties of high clouds on the radiation balance. The TOA upward components of the long-wave fluxes are slightly lower (except for ARM(B)) in 2D than 3D, by <2%; a greater mass of ice in layer cloud aloft provides increased absorption of infrared radiation emitted from the surface in 2D simulations.

The observed mean fluxes for TOGA-COARE and ARM are also shown in Table 2. For TOGA-COARE, two datasets for the observed radiative fluxes were utilized. Firstly, radiative fluxes at the top of the atmosphere were obtained from Patrick Minnis at NASA Langley. Minnis applies a relationship between narrowband radiances and broadband

TABLE 2. COMPARISONS OF LONG-WAVE AND SHORT-WAVE FLUXES AT THE TOP OF THE ATMOSPHERE (TOA) AND AT THE EARTH'S SURFACE (SFC) FOR SIMULATIONS AND OBSERVATIONS

Case	Simulations or observations	Short-wave flux (Wm^{-2})		Long-wave flux (Wm^{-2})	
		TOA upwards	SFC downwards	TOA upwards	SFC downwards
GATE	2D(X)	145.8	217.2	234.3	410.5
	2D(Y)	140.2	224.4	238.9	408.9
	3D	124.1	239.1	238.9	410.1
TOGA-COARE	2D(X)	193.1	147.3	179.4	428.4
	2D(Y)	185.7	163.0	177.4	419.8
	2D (long-domain)	177.2	167.0	182.3	425.9
	3D	183.2	158.8	179.6	427.9
	Observed (Minnis/IMET)	213.9	123.4	167.6	428.2
	Observed (ISCCP)	209.8	156.1	168.8	457.8
ARM (A)	2D(X)	139.3	300.7	257.1	370.6
	2D(Y)	124.3	327.3	263.9	369.4
	3D	120.4	323.4	262.8	370.3
	Observed	111.7	279.4	260.2	397.1
ARM (B)	2D(X)	123.7	316.9	261.0	373.7
	2D(Y)	138.0	296.6	258.7	377.4
	3D	128.6	308.0	259.1	377.0
	Observed	121.2	257.9	249.5	403.6
ARM (C)	2D(X)	133.2	302.8	253.8	376.7
	2D(Y)	123.3	313.2	257.7	375.1
	3D	127.5	305.9	253.8	378.0
	Observed	117.8	272.8	253.2	404.1

measurements (see Minnis *et al.* 1995). The surface fluxes of TOGA-COARE were obtained from IMET buoy data (see Burks 1998; Weller and Anderson 1996). Secondly, radiative fluxes were obtained from the International Satellite Cloud Climatology Project (ISCCP) (Zhang *et al.* 1995; Rossow and Zhang 1995). There are substantial discrepancies between these two sources of observed short-wave and long-wave fluxes. For ARM, observed radiative fluxes were obtained from the ARM web-site* (see also Xie *et al.* 2002).

In all TOGA-COARE runs, the albedo is slightly too low, with a tendency for the simulated TOA short-wave fluxes to be underestimated by about 10–20%. Consequently, the SFC downward short-wave fluxes are slightly overestimated. The long-wave fluxes are similarly accurate in TOGA-COARE. In all land cases, the TOA upward and SFC downward short-wave fluxes are too high by about 10%. The error in the upward TOA long-wave fluxes in the land cases is <4%, while the downward SFC long-wave flux is about 6% too low.

Errors in radiative fluxes predicted in the present study are comparable with errors from other CSRM studies. The UCLA/CSU† Cumulus Ensemble Model (CEM) simulation of an ARM intensive observing period case from 18 July to 3 August 1995 over the southern Great Plains, which was reported by Ghan *et al.* (2000), produced errors of a similar magnitude to those of simulations presented here. The 39-day simulation of TOGA-COARE by Wu *et al.* (1999) using a 2D CSRM produced an error

* <http://kiwi.atmos.colostate.edu:16080/scm/arm.html>

† University of California Los Angeles/Colorado State University.

of -13 W m^{-2} in the upward long-wave TOA flux and a percentage relative error in the fractional albedo of -5% , relative to the ISCCP data. This compares with a percentage relative error in the albedo, for the six-day simulation presented here, of -9% , which is probably higher because this period is more cloudy. The errors in surface fluxes predicted by Wu *et al.* are also comparable with results presented here.

For the land cases, the observed net short-wave absorption is $30\text{--}40 \text{ W m}^{-2}$ greater than predicted values. This error in the net short-wave absorption is comparable with the corresponding error (about 20 W m^{-2} , assuming a surface albedo of about 20%) for the UCLA/CSU CEM inferred from the study by Ghan *et al.* (2000). Ackerman *et al.* (2003) found no evidence of an excess of short-wave absorption in single-layer non-precipitating stratus decks below 3 km above MSL when comparing fluxes predicted by radiation models with observed fluxes. However, a comparison between their results and the integrations presented here is not possible because the WRF simulations generate considerably more complex cloud morphologies.

4. DISCUSSION AND CONCLUSIONS

In this study, evidence is presented for a significant sensitivity of predicted vertical velocities with respect to dimensionality. Related sensitivities of the cloud statistics of the microphysical and radiative processes to dimensionality are also found. These are consistent with weak ascent ($0.1 < w < \sim 1 \text{ m s}^{-1}$) being more prevalent outside deep convective updraughts in 2D compared with 3D. Such weak ascent outside the deep convective updraughts is less intense in 3D than in 2D, with vertical velocities being about 20% lower at each cumulative frequency.

The result from early modelling studies that deep convective updraughts are deeper and faster, whereas downdraughts are weaker, in 3D than in 2D (section 1) is qualitatively corroborated and extended to simulations of cases of cloud ensembles observed recently. Deep convective updraughts are $20\text{--}50\%$ faster at mid-levels in 3D than in 2D, while downdraughts are weaker by a similar fraction in the WRF runs. A partial exception in the present study is TOGA-COARE, for which WRF produces both faster downdraughts and more intense weak ascent in 3D than in 2D. In all cases the wind shear, despite being very different in the meridional and zonal directions, is found to produce much less impact on vertical-velocity statistics than the addition of a third dimension.

Statistics of cloud microphysics display a sensitivity to dimensionality that is consistent with the differences in updraught speed between 2D and 3D, especially in spatially extensive regions of shallow convection. Higher contents of cloud liquid and cloud ice are predicted in 2D compared with 3D in most cases. The relative slowness of weak ascent in 3D tends to reduce stratiform cloud relative to 2D. Graupel and snow contents tend to be lower and higher, respectively, by about $10\text{--}20\%$ and $10\text{--}70\%$, in 2D compared with 3D. The slow process of snow production is favoured in 2D because the stratiform cloud is more extensive than in 3D. Graupel production is favoured in 3D because the deep convective updraughts are more intense, upwelling a greater mass of rain and cloud liquid to subzero levels for freezing and riming, compared with 2D.

Whereas the thermodynamic response of deep convection to inclusion of the third dimension is quite similar between the present and previous studies (e.g. Grabowski *et al.* 1998; Donner *et al.* 1999), the sensitivities of fields of vapour and microphysical species differ substantially. The choice of microphysics scheme can drastically affect such sensitivities (Petch and Gray 2001). For WRF simulations of TOGA-COARE, the

lower and mid troposphere is drier in 2D than in 3D, especially with the long-domain 2D run. Qualitatively, this is consistent with results from Tompkins (2000) and Petch and Gray (2001). Donner *et al.* (1999) found that the main impact of the third dimension was to increase the intensity of the stratiform mesoscale circulation, with the maximum ratio of condensate to vapour being increased by 25%. This compares with an increase of almost 20% in the WRF simulations presented here.

Radiation in these WRF simulations is sensitive to dimensionality. Most of the changes are in the short wave and are related to changes in the microphysical properties of low cloud. Surface changes can exceed 20 W m^{-2} in the short wave. The predicted long-wave flux in WRF simulations is much less sensitive to dimensionality than is the short-wave flux because high cloud changes are less dependent on dimensionality. Furthermore, short-wave fluxes at the top of the atmosphere are predicted in most cases to be up to about 20 W m^{-2} higher in 2D(X) runs relative to 2D(Y).

Qualitatively, the salient features of the production of stratiform cloud in the melting layer seem quite realistic. Destabilization of the lower troposphere below the melting layer by melting-induced cooling was observed in several studies (Stewart *et al.* 1984; Willis and Heymsfield 1989). Similarly, in the WRF simulations, destabilization of the lower troposphere in stratiform regions is evident from the average profile of equivalent potential temperature. Sensitivity of the peak in cloud liquid content in the melting layer is partly related to convective destabilization in stratiform areas being greater in 2D than in 3D.

Land–ocean contrast is evident in the sensitivity to dimensionality in simulations presented here. In the upper troposphere above about 10 km there is a higher sensitivity of average updraught speeds over land. The fast updraughts reaching such high levels are particularly dimensionality-sensitive and occur more frequently over land. Convection over land is generally more intense, with higher peak rates of surface rainfall (section 2(c)). Also, the land cases display more sensitivity of the short-wave radiative flux to the choice of orientation of the vertical plane of 2D simulations than for the oceanic ones.

The sensitivity with respect to dimensionality is somewhat different in TOGA-COARE. Weak ascent is more frequent at most vertical velocities above 8 km in 3D compared with 2D for this case. Consequently, descent is also more frequent at most vertical velocities. Redelsperger *et al.* (2000) also found that downdraughts are faster in 3D than in 2D in a TOGA-COARE case. In WRF simulations of TOGA-COARE, production of anvil cloud is greater, with a peak content of cloud ice that is at least three times as high, than in the other cases owing to high humidity in the mid and upper troposphere (section 2(c)). Previous studies have shown that the third dimension acts to increase the turbulent circulations associated with radiative cooling in such anvil clouds (e.g. Petch and Gray 2001), which favours weak ascent being more prevalent in 3D than in 2D.

Finally, the WRF simulations have domains comparable in size and resolution with that of a CSRM super-parametrization (e.g. Khairoutdinov and Randall 2001). The WRF results imply that a 2D super-parametrization would be biased in its prediction of radiative fluxes by the lack of a third dimension by up to 20 W m^{-2} in regions of deep convection. Additionally, the microphysical properties depend strongly on dimensionality, and this would have large impacts on attempts to simulate the aerosol–cloud interaction (the indirect effect). Although not considered here, the transport of horizontal momentum depends critically on dimensionality, and this dependency opens a wide range of additional issues related to CSRM dimensionality in super-parametrization.

REFERENCES

- Ackerman, T. P., Flynn, D. M. and Marchand, R. T. 2003 Quantifying the magnitude of anomalous solar absorption. *J. Geophys. Res.*, **108**, D9, 4273, doi: 10.1029/2002JD002674
- Atlas, D. 1955 'The origin of stalactites in precipitation echoes'. Pp. 321–326 in Proceedings of the weather radar conference, Asbury Park NJ, USA, September 1955. US Army Signal Corps, Fort Monmouth NJ, USA
- Atlas, D., Tatehia, R., Srivastava, R. C., Marker, W. and Carbone, R. E. 1969 Precipitation-induced mesoscale wind perturbations in the melting layer. *Q. J. R. Meteorol. Soc.*, **95**, 544–560
- Burks, J. E. 1998 'Radiative fluxes and heating rates during TOGA-COARE over the Intensive Flux Array'. MSc dissertation, University of Utah, USA
- Ciesielski, P. E., Hartten, L. M. and Johnson, R. H. 1997 Impacts of merging profiler and rawinsonde winds on TOGA-COARE analyses. *J. Atmos. Ocean. Technol.*, **14**, 1264–1279
- Cotton, W. R. and Tripoli, G. J. 1978 Cumulus convection in shear flow—three-dimensional numerical experiments. *J. Atmos. Sci.*, **35**, 1503–1521
- Donner, L. J., Seman, C. J. and Hemler, R. S. 1999 Three-dimensional cloud-system modeling of GATE convection. *J. Atmos. Sci.*, **56**, 1885–1912
- Dyer, A. J. and Hicks, B. B. 1970 Flux-gradient relationships in the constant flux layer. *Q. J. R. Meteorol. Soc.*, **96**, 715–721
- Findeisen, W. 1940 The formation of the 0 degC isothermal layer and fractocumulus under nimbostratus. *Meteorol. Z.*, **57**, 49–54
- Freidenreich, S. M. and Ramaswamy, V. 1999 A new multiple-band solar radiative parameterization for general circulation models. *J. Geophys. Res.*, **104**, 31389–31410
- Fu, Q. and Liou, K. N. 1993 Parameterization of the radiative properties of cirrus clouds. *J. Atmos. Sci.*, **50**, 2008–2025
- Fu, Q., Krueger, S. K. and Liou, K. N. 1995 Interactions of radiation and convection in simulated tropical cloud clusters. *J. Atmos. Sci.*, **52**, 1310–1328
- Ghan, S. J., Randall, D. A., Xu, K.-M., Cederwall, R. T., Cripe, D. G., Hack, J., Iacobellis, S. F., Klein, S. A., Krueger, S. K., Lohmann, U., Pedretti, J., Robock, A., Rotstayn, L. D., Somerville, R. C., Stenchikov, G., Sud, Y. C., Walker, G. K., Xie, S. C., Yio, J. J. and Zhang, M.-H. 2000 A comparison of single column model simulations of summertime midlatitude continental convection. *J. Geophys. Res.*, **105**, D2, 2091–2124
- Grabowski, W. W. 2001 Coupling cloud processes with the large-scale dynamics using the cloud-resolving convection parameterization (CRCP). *J. Atmos. Sci.*, **58**, 978–997
- Grabowski, W. W. and Smolarkiewicz, P. K. 1999 CRCP: A cloud resolving convection parameterization for modeling the tropical convecting atmosphere. *Physica D*, **133**, 171–178
- Grabowski, W. W., Wu, X. and Moncrieff, M. W. 1996 Cloud resolving modeling of tropical cloud systems during Phase III of GATE. Part I: Two-dimensional experiments. *J. Atmos. Sci.*, **53**, 3684–3709
- Grabowski, W. W., Wu, X., Moncrieff, M. W. and Hall, W. D. 1998 Cloud-resolving modeling of cloud systems during Phase III of GATE. Part II: Effects of resolution and the third spatial dimension. *J. Atmos. Sci.*, **55**, 3264–3282
- Held, I., Hemler, R. S. and Ramaswamy, V. 1993 Radiative-convective equilibrium with explicit two-dimensional moist convection. *J. Atmos. Sci.*, **50**, 3909–3927
- Heymsfield, A. J. and Donner, L. J. 1990 A scheme for parameterizing ice-cloud water content in general circulation models. *J. Atmos. Sci.*, **47**, 1865–1877
- Heymsfield, A. J., Miloshevich, L. M., Schmitt, C., Bansemer, A., Twohy, C., Poellot, M. R., Fridlind, A. and Gerber, H. 2005 Homogeneous ice nucleation in subtropical and tropical convection and its influence on cirrus anvil microphysics. *J. Atmos. Sci.*, **62**, 41–65
- Hong, S.-Y. and Pan, H.-L. 1996 Nonlocal boundary layer vertical diffusion in a medium-range forecast model. *Mon. Weather Rev.*, **124**, 2322–2339
- Khairoutdinov, M. and Randall, D. A. 2001 A cloud resolving model as a cloud parameterization in the NCAR Community Climate System model: Preliminary results. *Geophys. Res. Lett.*, **28**, 3617–3620

- LeMone, M. A. and Zipser, E. J. 1980 Cumulonimbus vertical velocity events in GATE. Part I: Diameter, intensity and mass flux. *J. Atmos. Sci.*, **37**, 2444–2457
- Lin, Y.-L., Farley, R. D. and Orville, H. D. 1983 Bulk parameterization of the snow field in a cloud model. *J. Climate Appl. Meteorol.*, **22**, 1065–1092
- Lipps, F. B. and Hemler, R. 1986 Numerical simulation of deep tropical convection associated with large-scale convergence. *J. Atmos. Sci.*, **43**, 1796–1816
- Lord, S. J., Willoughby, H. E. and Piotrowicz, J. M. 1984 Role of a parameterized ice-phase microphysics in an axisymmetric nonhydrostatic tropical cyclone model. *J. Atmos. Sci.*, **41**, 2836–2848
- McFarquhar, G. M., Heymsfield, A. J., Macke, A., Iaquinta, J. and Aulenbach, S. M. 1999 Use of observed ice crystal sizes and shapes to calculate mean-scattering properties and multispectral radiances: CEPEX April 4 1993 case study. *J. Geophys. Res.*, **104**, D24, 31763–31779
- Michalakes, J., Chen, S., Dudhia, J., Hart, L., Klemp, J., Middlecoff, J. and Skamarock, W. 2001 ‘Development of a next generation regional weather research and forecast model’. Pp. 269–276 in Proceedings of the ninth ECMWF workshop on the use of high performance computing in meteorology—Developments in Teracomputing, Eds. Walter Zwiefelhofer and Norbert Kreitz. World Scientific, Singapore
- Minnis, P., Smith, W. L., Garber, D. P., Ayers, J. K. and Doelling, D. R. 1995 ‘Cloud properties derived from GOES-7 for spring 1994 ARM intensive observation period using version 1.0.0 of ARM satellite data analysis program’. NASA reference publication 1366
- Moeng, C.-H., Cotton, W. R., Bretherton, C., Chlond, A., Khairoutdinov, M., Krueger, S., Lewellen, W. S., MacVean, M. K., Pasquier, J. R. M., Rand, H. A., Siebesma, A. P., Stevens, B. and Sykes, R. I. 1996 Simulation of the stratocumulus-topped planetary boundary layer: Intercomparison among different numerical codes. *Bull. Am. Meteorol. Soc.*, **77**, 261–278
- Moore, G. W. and Stewart, R. E. 1985 The coupling between melting and convective air motions in stratiform clouds. *J. Geophys. Res.*, **90**, D6, 10659–10666
- Paulson, C. A. 1970 The mathematical representation of wind speed and temperature profiles in the unstable atmospheric surface layer. *J. Appl. Meteorol.*, **9**, 857–861
- Petch, J. C. and Gray, M. E. B. 2001 Sensitivity studies using a cloud-resolving model simulation of the tropical west Pacific. *Q. J. R. Meteorol. Soc.*, **127**, 2287–2306
- Phillips, V. T. J., Donner, L. J. and Garner, S. 2006 Nucleation processes in deep convection simulated by a cloud-system resolving model with double-moment bulk microphysics. *J. Atmos. Sci.* (in press)
- Redelsperger, J. L., Brown, P. R. A., Guichard, F., Hoff, C., Kawasima, M., Lang, S., Montmerle, T., Nakamura, K., Saito, K., Seman, C., Tao, W. K. and Donner, L. J. 2000 A GCMSS model intercomparison for a tropical squall line observed during TOGA-COARE. I: Cloud-resolving models. *Q. J. R. Meteorol. Soc.*, **126**, 823–863
- Riehl, H. 1977 Venezuelan rain systems and the general circulation of the summer tropics: Rain systems. *Mon. Weather Rev.*, **105**, 1402–1420
- Rossow, W. B. and Zhang, Y.-C. 1995 Calculation of surface and top of atmosphere radiative fluxes from physical quantities based on ISCCP datasets. 2. Validation and first results. *J. Geophys. Res.*, **100**, 1167–1197
- Savijarvi, H. 1997 Shortwave optical properties of rain. *Tellus*, **49a**, 177–181
- Savijarvi, H., Arola, A. and Raisanen, P. 1997 Short-wave optical properties of precipitating water clouds. *Q. J. R. Meteorol. Soc.*, **123**, 883–899
- Schlesinger, R. E. 1984 Effects of the pressure perturbation field in numerical models of unidirectionally sheared thunderstorm convection: Two versus three dimensions. *J. Atmos. Sci.*, **41**, 1571–1587
- Schwarzkopf, M. D. and Ramaswamy, V. 1999 Radiative effects of CH₄, N₂O halocarbons and the foreign-broadened H₂O continuum: A GCM experiment. *J. Geophys. Res.*, **104**, 9467–9488
- Slingo, A. 1989 A GCM parameterization for the shortwave radiative properties of water clouds. *J. Atmos. Sci.*, **46**, 1419–1427
- Stewart, R. E., Marwitz, J. D., Pace, J. C. and Carbone, R. E. 1984 Characteristics through the melting layer of stratiform clouds. *J. Atmos. Sci.*, **41**, 3227–3237

- Su, H., Chen, S. S. and Bretherton, C. S. 1999 Three-dimensional week-long simulations of TOGA-COARE convective systems using the MM5 mesoscale model. *J. Atmos. Sci.*, **56**, 2326–2343
- Tag, P. M. and Rosmond, T. E. 1980 Accuracy and energy conservation in a three-dimensional anelastic model. *J. Atmos. Sci.*, **37**, 2150–2160
- Tao, W.-K., Simpson, J. and Soong, S.-T. 1987 Statistical properties of a cloud ensemble: A numerical study. *J. Atmos. Sci.*, **44**, 3175–3187
- Thompson, R. M., Payne, S. W., Recker, E. E. and Reed, R. J. 1979 Structure and properties of synoptic-scale wave disturbances in the intertropical convergence zone of the eastern Atlantic. *J. Atmos. Sci.*, **36**, 53–72
- Tompkins, A. M. 2000 The impact of dimensionality on long-term cloud-resolving model simulations. *Mon. Weather Rev.*, **128**, 1521–1535
- Webb, E. K. 1970 Profile relationships: The log-linear range, and extension to strong stability. *Q. J. R. Meteorol. Soc.*, **96**, 67–90
- Weller, R. A. and Anderson, S. P. 1996 Surface meteorology and air–sea fluxes in the western equatorial Pacific warm pool during the TOGA Coupled Ocean–Atmosphere Response Experiment. *J. Climate*, **9**, 1959–1990
- Wexler, R., Reed, R. J. and Honig, J. 1954 Atmospheric cooling by melting. *Bull. Am. Meteorol. Soc.*, **35**, 48–51
- Wicker, L. J. and Skamarock, W. C. 2002 Time-splitting methods for elastic models using forward time schemes. *Mon. Weather Rev.*, **130**, 2088–2097
- Wilhelmson, R. 1974 The life cycle of a thunderstorm in three dimensions. *J. Atmos. Sci.*, **31**, 1629–1651
- Willis, P. T. and Heymsfield, A. J. 1989 Structure of the melting layer in mesoscale convective system stratiform precipitation. *J. Atmos. Sci.*, **46**, 2008–2025
- Wu, X., Hall, W. D., Grabowski, W. W., Moncrieff, M. W., Collins, W. D. and Kiehl, J. T. 1999 Long-term behavior of cloud systems in TOGA COARE and their interactions with radiative and surface processes. Part II: Effects of ice microphysics on cloud–radiation interaction. *J. Atmos. Sci.*, **56**, 3177–3195
- Xie, S., Xu, K.-M., Cederwall, R. T., Bechtold, P., Del Genio, A. D., Klein, S. A., Cripe, D. G., Ghan, S. J., Gregory, D., Jacobellis, S. F., Krueger, S. K., Lohmann, U., Petch, J. C., Rotstayn, L. D., Randall, D. A., Somerville, R. C., Sud, Y. C., Salzen, K., Walker, G. K., Wolf, A., Yio, J. J., Zhang, G. J. and Zhang, M.-H. 2002 Intercomparison and evaluation of cumulus parametrizations under summertime midlatitude continental conditions. *Q. J. R. Meteorol. Soc.*, **128**, 1095–1135
- Xu, K.-M. 1995 Partitioning mass, heat, and moisture budgets of explicitly simulated cumulus ensembles into convective and stratiform components. *J. Atmos. Sci.*, **52**, 551–573
- Xu, K.-M., Cederwall, R. T., Donner, L. J., Grabowski, W. W., Guichard, F., Johnson, D. E., Khairoutdinov, M., Krueger, S. K., Petch, J. C., Randall, D. A., Seman, C. J., Tao, W.-K., Wang, D., Xie, S. C., Yio, J. J. and Zhang, M.-H. 2002 An intercomparison of cloud-resolving models with the Atmospheric Radiation Measurement summer 1997 intensive observations period data. *Q. J. R. Meteorol. Soc.*, **128**, 593–624
- Zhang, M. H. and Lin, J. L. 1997 Constrained variational analysis of sounding data based on column-integrated budgets of mass, heat, moisture, and momentum: Approach and application to ARM measurements. *J. Atmos. Sci.*, **54**, 1503–1524
- Zhang, M. H., Lin, J. L., Cederwall, R. R., Yio, J. J. and Xie, S. C. 2001 Objective analysis of ARM IOP data: Method and sensitivity. *Mon. Weather Rev.*, **129**, 295–311
- Zhang, Y.-C., Rossow, W. B. and Lacis, A. A. 1995 Calculation of surface and top of atmosphere radiative fluxes from physical quantities based on ISCCP datasets. 1. Method and sensitivity to input data uncertainties. *J. Geophys. Res.*, **100**, 1149–1166